Title

Tensor Tomography of Dark Field Scatter using X-ray Interferometry with Bi-prisms

Authors

Gullberg, Grant T

Fuller, Michael

Shrestha, Uttam

et al.

Publication Date

2017-10-01

DOI

10.1109/nssmic.2017.8533088

Peer reviewed

Published in final edited form as:

IEEE Nucl Sci Symp Conf Rec (1997). 2017 October ; 2017: . doi:10.1109/NSSMIC.2017.8533088.

Tensor Tomography of Dark Field Scatter using X-ray Interferometry with Bi-prisms

Grant T. Gullberg [Fellow, IEEE],
Department of Radiology and Biomedical Imaging, University of California San Francisco, 94143-0946 USA (gtgullberg@lbl.gov)

Michael Fuller,
TF Instruments, Salinas, CA USA (michael.fuller@tfinstruments.com)

Uttam Shrestha, and
Department of Radiology and Biomedical Imaging, University of California San Francisco, 94143-0946 USA (uttam.shrestha@ucsf.edu)

Youngho Seo [Senior Member, IEEE]
Department of Radiology and Biomedical Imaging, University of California San Francisco, 94143-0946 USA (youngho.seo@ucsf.edu).

Abstract

X-ray grating-based differential phase-contrast imaging is able to obtain excellent soft-tissue contrast of phase, attenuation, and small angle scatter. In this work we model the performance of an X-ray interferometer wherein the phase gratings are replaced with a single Fresnel micro-bi-prism. Our goal is to develop imaging systems based on bi-prism interferometry with improved polychromatic performance. In our investigation we obtain an analytical expression for the irradiance distribution of the bi-prism. The localized regions of fringe visibility within the irradiance distribution are non-periodic. Following the work of Pfeiffer et al., we then develop a method for reconstructing scattering directions that can be used to obtain a three-dimensional tensor field. This will eventually be used in modified bi-prism-based differential phase-contrast imaging to obtain tissue properties through mathematical reconstruction of tensor tomographic data.

I. Introduction

X-ray CT is the foundation of the medical imaging industry. However, medical imaging has not taken full advantage of its potential to measure tissue properties that are possible by measuring and modeling the full extent of the physics involved in the interaction of X-rays with soft tissue. To obtain measures of the full tissue properties, one needs to develop imaging systems that can provide highly resolved X-rays with spatially-modulated intensity. This can be accomplished using diffraction gratings and bi-prisms. This modulation is feasible even with a conventional X-ray tube by using a Talbot-Lau interferometer most often coupled with gratings for differential phase-contrast imaging (DPCI) [1]. The same could be achieved using bi-prisms in which there are no optics in the X-ray beam between the sample and the detector [2]. Such postexposure gratings cause loss of detected X-rays

leading to higher radiation absorbed dose, and present optical alignment challenges. Interferometry-based X-ray imaging has provided excellent soft-tissue contrast [3] of phase, attenuation, and small angle scatter information of tissue properties.

In our investigation, it is proposed that the Fresnel bi-prism [4,5] be used to produce high-contrast fringes with spatially incoherent X-ray illumination. The bi-prism array interferometer improves the signal-to-noise ratio of the original signal and provides a means to measure phase-shifts of introduced objects. In addition to developing imaging systems based on bi-prism-based interferometry, we propose to develop algorithms for tomographic reconstructions from projections of phase contrast data to retrieve images of absorption, differential phase, and dark field small-angle scatter. In this work, we focus on the reconstruction of small angle scatter.

We first develop an analytical expression for the irradiance distribution of the bi-prism. Then using the work of Pfeiffer et al. [6], [7], [8], [9], we develop analytical expressions for the projections of a finite set of fixed scattering directions at each voxel in space. Using the developed analytical expression of the irradiance distribution, we provide results for 17.5 keV X-rays demonstrating irradiance distributions for different number of point sources, point source separations, and bi-prism angles.

II. Methods

A. Grating Interferometry with a Bi-prism

In this paper, it is proposed that the Fresnel bi-prism be used to produce high-contrast fringes with spatially incoherent X-ray illumination (Fig. 1). X-rays refracting through each prism element overlap and form divergent (magnified) interference fringes on a distant detector. A further advantage when using polychromatic radiation is that the central fringe produced by a bi-prism is always a “white light” fringe. We propose a modified X-ray interferometer [1] wherein the phase grating (G1) is replaced with an array of Fresnel micro-biprisms. Also, a novel design for the source grating (G0) is provided and the analyzer grating (G2) might be eliminated. our analysis in this paper is performed on a single set of two counter-positioned refractive prisms illuminated with multiple sources.

B. Analytical Expression for the Irradiance Distribution

Assuming an x-ray beam proceeding from a spatially incoherent planar source illuminates a thin bi-prism, we write the irradiance distribution on an arbitrary plane placed at a distance z beyond the bi-prism as [4]

$$I(\overrightarrow{x}, z; \eta) = \frac{1}{M_S^2} I_S\left(\frac{\overrightarrow{x}}{M_S}\right) \otimes_2 I_0(\overrightarrow{x}, z; \eta), \quad (1)$$

where η is the distance between the source and the bi-prism, z is the distance between the bi-prism and the imaging plane, $\otimes_2$ is the 2D convolution performed over the transverse coordinates $\overrightarrow{x} = (x, y)$, I_S is the irradiance distribution of the planar source, I_0 is the

irradiance distribution of the Fresnel biprism, I is the irradiance distribution at the observation plane, and $M_S = -z/\eta$ is the magnification factor between the source and the observation planes.

For a spherical wavefront proceeding from a point source illuminating a Fresnel bi-prism, the exiting wavefront produces an interference pattern beyond the Fresnel bi-prism whose irradiance distribution is

$$I_0(\vec{x}, z; \eta) = 1 + cos\left(\frac{2\pi x}{p}\right),$$

where $p = \lambda(\eta + z)/(2\eta tan\alpha)$ is the period of the interference pattern, $\alpha = \delta tan\chi$ is the angle of the beam deflection [5], δ is the refraction index decrement, and χ is the angle of the biprism (Fig. 2). Here we differ from the development in [4] for light in changing $p = \lambda(\eta + z)/(2(n-1)\eta\theta)$, where n is the index of refraction and θ is the refringence angle of the bi-prism given in [4], to $p = \lambda(\eta + z)/(2\eta tan\alpha)$ where $\alpha = \delta\tan(\chi)$ is shown in Fig. 2.

For the case of special interest in which the quasi-monochromatic source is composed by an array of N mutually incoherent point sources with the same irradiance, I_P, and arranged equidistant perpendicular to the bi-prism edge and distributed symmetrically to the optical axis, the irradiance distribution of the sources is

$$I_S(\vec{x}) = \sum_{i=1}^{N} I_P \delta(x - x_i, y),$$
$$x_i = \left(\frac{N+1}{2} - i\right)x_0, i = 1, \ldots\ldots, N,$$

x_0 being the separation between neighbor point sources. By using Eq. (1), the irradiance distribution is obtained to be as follows:

$$I(\vec{x}, z; \eta) = I_P \sum_{i=1}^{N} I_0(x - M_S x_i, y, z; \eta).$$

In a realistic experimental situation, the width Δ of the sources along the x direction would not be infinitesimal. In that case, the irradiance distribution of the source can be written as the convolution between $I_S(\vec{x})$ and a rectangle of width Δ. Using Mathematica (Wolfram Research, Champaign, Illinois), we come up with the following analytical expression:

$$If\ N = 1 \qquad I(x,z) = I_P\left(\Delta^2 + \frac{1}{2\pi z tan\alpha}\lambda\,\Delta\,(z+\eta)cos\left[\frac{4\pi x\eta tan\alpha}{\lambda(z+\eta)}\right]sin\left[\frac{2\pi\,\Delta\,z tan\alpha}{\lambda(z+\eta)}\right]\right),$$

$$If\ N > 1\ \ I(x,z) = I_P\left(N\,\Delta^2 + \frac{1}{2\pi z tan\alpha}\lambda\,\Delta\,(z+\eta)cos\left[\frac{4\pi x\eta tan\alpha}{\lambda(z+\eta)}\right]sin\left[\frac{2\pi\,\Delta\,z tan\alpha}{\lambda(z+\eta)}\right]CSC\left[\frac{2\pi x_0 z tan\alpha}{\lambda(z+\eta)}\right]sin\left[\frac{2N\pi x_0 z tan\alpha}{\lambda(z+\eta)}\right]\right)$$

(2)

C. Model of Scatter for Dark Field Projections

Here we develop a model of scatter presented in dark field projections. We assume an X-ray beam proceeds from a spatially incoherent planar source and illuminates a thin biprism emitting an irradiance distribution projected onto an object of interest. If we assume a fixed finite number of scattering directions $\epsilon_k = \zeta_k(x)\hat{\epsilon}_k \in \mathbb{R}^3$, from the work in [6,7] we write the projections of the dark field image as,

$$d_j = exp\left[-\int_{L_j} \Sigma_k \left\langle \mid \hat{l}_j \times \hat{\epsilon}_k \mid \zeta_k(x)\hat{\epsilon}_k, t_j \right\rangle^2 dx\right], \quad (3)$$

where $\hat{l}_j \in \mathbb{R}^3$ is the direction of the incoming beam, L_j is the line along this direction, and $t_j = \mid t_j \mid \hat{t}_j \in \mathbb{R}^3$ is the sensitivity direction parallel to the detector surface. The ^ indicates a unit vector. One can show that this reduces to

$$d_j = exp\left[-\sum_k \nu_{kj} \int_{L_j} \eta_k(x) dx\right],$$

where $\eta_k(x) = \zeta_k(x)^2$ and $v_{kj} = \mid t_j \mid^2 \mid \hat{l}_j \times \hat{\epsilon}_k \mid^2 \left\langle \hat{\epsilon}_k, \hat{t}_j \right\rangle^2$. The $\eta_k(x)$ at the position x are the square of the coefficients of the vector scattering directions $\hat{\epsilon}_k$.

Let's parameterize the X-ray direction [8] so that we replace j with $i,j,\theta_q,\phi_r,\omega_s$, such that the capital letters I, J, Q, R, S are the dimensions for each coordinate. Defining the detector elements with coordinates (i,j) and the projection angles of the sample as θ_q,ϕ_r,ω_s as shown in Fig. 3, then

$$D(i,j,\theta_q,\phi_r,\omega_s) = exp\left[-\sum_k v_{kijqrs} \int_{L_{ijqrs}} \eta_k(x) dx\right].$$

We can form the reconstruction problem as the solution to a large system of linear equations

$$m = (m_{ijqrs}) = \left(-ln(D(i,j,\theta_q,\phi_r,\omega_s)\right) = H\eta$$

where $H = (D_1A, D_2A, \ldots, D_KA)$ is a J×IK matrix, and

$$D_k = \begin{pmatrix} v_{k1} & \cdots & 0 \\ \vdots & \ddots & \vdots \\ 0 & \cdots & v_{kIJQRS} \end{pmatrix}$$

is a IJQRS×IJQRS diagonal matrix of weighting coefficients v_{kijqrs}, IJQRS is the number of projection samples, NMP is the number of voxels in the 3D array, K is the number of scattering directions $\hat{\epsilon}_k$, and

$$\eta^T = (\eta_{11}, \eta_{12}, \ldots, \eta_{1NMP}, \eta_{21}, \eta_{22}, \ldots, \eta_{2NMP}, \ldots \ldots, \eta_{K1}, \eta_{K2}, \ldots, \eta_{KNMP})$$

is a NMPK×1 matrix of unknown coefficients to be determined. A is the system matrix of the tomographic projections formed by the integral in the above equations.

Writing the matrix formulation of the system of equations explicitly in terms of the unknown coefficients η_{ij}, we have

$$m = H\eta = \overbrace{(D_1 A, D_2 A, \ldots D_K A)}^{IJQRS \times KNMP} \overbrace{\begin{pmatrix} \eta_{11} \\ \vdots \\ \eta_{1NMP} \\ \eta_{21} \\ \eta_{22} \\ \vdots \\ \eta_{2NMP} \\ \vdots \\ \eta_{K1} \\ \eta_{K2} \\ \vdots \\ \eta_{KNMP} \end{pmatrix}}^{KNMP \times 1}. \quad (4)$$

D. Processing Dark Field Projections

The projection of the bi-prism irradiance distribution onto the detector surface is a periodic pattern (Fig. 9). We can approximate the Fourier expansion as [9]

$$I(i, j, \theta_q, \phi_r, \omega_s, x_g) \approx a_0(i, j, \theta_q, \phi_r, \omega_s) + a_1(i, j, \theta_q, \phi_r, \omega_s \quad (5)$$
$$)\cos\left[\frac{2\pi(i - (I+1)/2)}{x_p} x_s - \ \Phi\ (i, j, \theta_q, \phi_r, \omega_s)\right],$$

where (i,j) are coordinates of the detector pixel; x_s is the spatial sampling; x_p is the period in x; θ_q, ϕ_r, ω_s is the rotation angle of the sample around the optical axis; and a_0, a_1, and Φ are the mean, amplitude, and phase of the sinusoidal curve, respectively. Defining the visibility of the scatter and reference signal as

$$V^{s/r}(i,j,\theta_q,\phi_r,\omega_s) = a_1^{s/r}(i,j,\theta_q,\phi_r,\omega_s)/a_0^{s/r}(i,j,\theta_q,\phi_r,\omega_s).$$

The dark field scatter signal is the following ratio of normalized visibilities

$$V(i,j,\theta_q,\phi_r,\omega_s) = V^s(i,j,\theta_q,\phi_r,\omega_s)/V^r(i,j,\theta_q,\phi_r,\omega_s).$$

III. Results

MathCad (Parametric Technology Corporation, Needham, Massachusetts) was used to numerically evaluate Eq. (2) to obtain fringe patterns behind the bi-prism for incoherent X-ray point sources located at $\eta = 0.4$ m in front of the bi-prism (see Fig. 1). For the calculation we set $\lambda = 7.1 \times 10^{-11}$m, $Ip = 1/\Delta^2$, $\Delta = 7.00 \times 10^{-7}$, and $\alpha = \delta\tan(\chi)$, where $\delta = 1.57 \times 10^{-6}$. Using these parameters a series of calculations was made for different number of point sources, point source separations, and bi-prism angles.

Fig. 4 shows the fringe pattern for one point source with a biprism angle of χ=82°. Fig. 5 shows the fringe pattern for two point sources separated by $x_0 = 20$ μm with a bi-prism angle of χ=82°. Note that for a scale of 0 to 2 for one point source the scale ranges from 0 to 4 for two point sources. Therefore, the scale increases in proportion to the number of point sources as is seen with a scale of 0 to 50 for 25 point sources in Figs. 6, 7, and 8.

Non-periodic visibility is seen in Fig. 6. This is characteristic of fringe visibility for a bi-prism and differs from the periodic pattern of the well-known Talbot–Lau interferometer coupled with gratings. Figs. 6 and 7 demonstrate the sensitivity of reducing the distance from $x_0 = 36.7$ μm to $x_0 = 3.67$ μm between the point sources. Also notice in Figs. 7 and 8 the sensitivity of increasing the bi-prism angle from χ=82° to χ=83.67°.

Finally using Eq. (2) we plotted in Fig. 9 the projection of the bi-prism irradiance distribution onto the detector surface at 0.9 m for 25 point sources separated by $x_0 = 3.67$ μm and with a bi-prism angle of χ=83.67°. The full width at half maximum of the central beam at 0.9 meters is approximately 6 μm. Notice the periodicity of the amplitude of the central fringe which can be modeled by the Fourier expansion in Eq. (5).

IV. Discussion

Here we present an approach for obtaining tomographic dark field images from projections of X-ray small angle scatter. Our presentation of the equations follows closely the work of the group of Pfeiffer [6], [7], [8], [9]. However our approach differs in that we propose to use bi-prisms instead of gratings. The possible benefits of this approach are **1)** Greater optic-to-detector distance allows placement of the sample/patient after the bi-prism array; **2)** Divergent nature of the bi-prism's fringes allows detection in a single exposure (Moiré pattern); **3)** Setup is well suited to commercially available multi-spot X-ray sources; **4)** Better use of a polychromatic X-ray spectrum by the naturally varied offset (wavelength

dependent) of the bi-prism's virtual sources; and **5)** Easier manufacturing, straight-forward alignment, and improved throughput.

Please note the geometry implied in Figs. 6 and 9. The overall distance of X-ray source-to-X-ray detector of 1.3-meters corresponds to commercially available CT systems (large bore systems). This presumes possible retrofit of a bi-prism array to certain clinical imaging equipment. Another future possibility would be a highly modified cone-beam CT setup where the source grating and bi-prism array are simultaneously rotated around the beam-axis, defined by the point source, gantry isocenter, and center of area detector. such a setup would provide multi-axis and multi-view vector scattering data, which would allow for analysis of tissue microstructure orientation, elastomeric properties, and perfusion bias – all known health indictors.

As with the work in [7], at every image voxel a fixed set of scatter vector directions is assumed for which the coefficients are estimated from the measured projections in Eq. (3). The tomographic projections in Eq. (3) are projections of the amplitudes of the scattering directions. solving the system of equations in Eq. (4), provides estimates of these coefficients. This is accomplished by forming a likelihood function assuming the detection of photons follows a Poisson distribution. The estimates of the coefficients are obtained by maximizing the likelihood function using the expectation maximization (EM) algorithm. A tensor at each voxel is obtain by fitting the weighted fixed set of vectors to ellipsoids [6], [7].

Heretofore, the X-ray beam in a CT system has been emitted from a single, relatively large spot origin and has not had spatial coherence per say. This has kept CT systems from recording sample features that cause phase-shift or small-angle forward-scatter in the transmitted x-rays. Such features are often related to tissue health but can only be observed with illuminating X-rays of high spatial resolution – that is, rays that are highly resolved in space. One method of breaking up the full field of X-radiation is by using a Talbot–Lau interferometer, using multiple gratings for differential phase-contrast imaging (DPCI) [1]. The same could be achieved using bi-prisms coupled only to a source grating with which there are no optics in the x-ray beam between the sample and the detector, a significant improvement over grating-based interferometers [2]. We feel that bi-prism-based interferometry has the potential to revolutionize phase-contrast and dark-field X-ray CT.

Acknowledgments

This work was supported in part by the National Institutes of Health under Grant Nos. R01 EB012965 and R01 HL135490.

References

[1]. Pfeiffer F, Kottler C, Bunk O, and David C, "Hard x-ray phase tomography with low-brilliance sources," Phys. Rev. Lett, vol. 98, 108105, 2007. [PubMed: 17358572]

[2]. Gullberg GT, Fuller M, Shrestha U, Seo Y, "Irradiance distribution of an x-ray source illuminating bi-prism gratings," 4th International Conference on X-ray and Neutron Phase Imaging with Gratings (XNPIG2017), Zurich, Switzerland, September 12-15, 2017.

[3]. Pfeiffer F, Bunk O, David C, Bech M, Duc GL, Bravin A, and Cloetens P, "High resolution brain tumor visualization using three-dimensional x-ray phase contrast tomography," Phys. Med. Biol, vol. 52, 6923, 2007. [PubMed: 18029984]

[4]. Doblas A, Saavedra G, Martinez-Corral M, Barreiro JC, Sanchez-Ortiga E, and Llavador A, “Axial resonance of periodic patterns by using a Fresnel biprism,” J. Opt. Soc. Am. A, vol. 30, 140, 2013.

[5]. Ablett JM, Evans-Lutterodt K, and Stein A, “Hard x-rays Fresnel prisms: Properties and applications,” in Design and Microfabrication of Novel X-ray Optics II, Snigirev AA and Mancini DC, Eds. Proceedings of SPIE, vol. 5539, 8 2, 2004.

[6]. Malecki A, Potdevin G, Biernath T, Eggl E, Willer K, Lasser T, Maisenbacher J, Gibmeier J, Wanner A, and Pfeiffer F, “X-ray tensor tomography,” EPL (Europhysics Letters), vol. 105, no. 3, pp. 38002, 2014.

[7]. Vogel J, Schaff F, Fehringer A, Jud C, Wieczorek M, Pfeiffer F, and Lasser T, “Constrained X-ray tensor tomography,” Opt Express, vol. 23, no. 12, pp. 15134–51, 2015. [PubMed: 26193497]

[8]. Sharma Y, Wieczorek M, Schaff F, Seyyedi S, Prade F, Pfeiffer F, and Lasser T, “Six dimensional X-ray Tensor Tomography with a compact laboratory setup,” Appl. Phys. Lett Vol. 109, 134102, 2016.

[9]. Jensen TH, Bech M, Bunk O, Donath T, David C, Feidenhans IR, and Pfeiffer F, « Directional x-ray dark-field, imaging,” Phys. Med. Biol, vol. 55, pp. 3317–3323, 2010. [PubMed: 20484780]

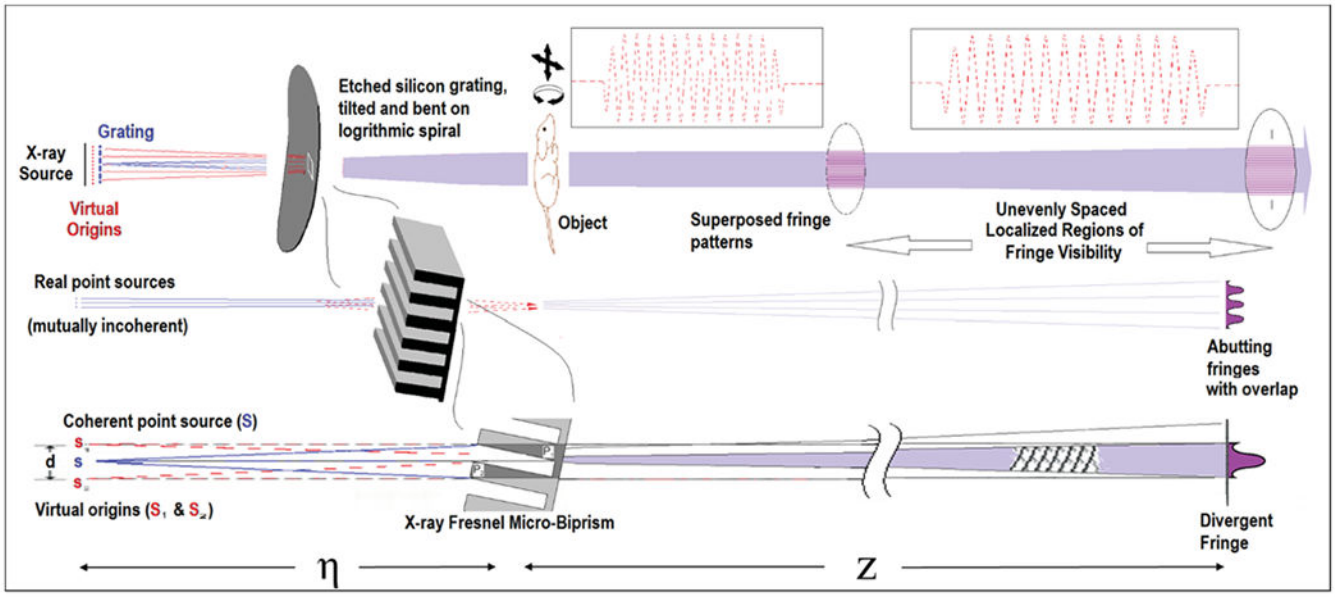

Fig. 1.

Schematic diagram of X-ray optical approach, showing overall setup (top), expanded view of bi-prism array (middle) with multiple X-ray origins each producing fringes in resonant position, and operation of a single bi-prism with one X-ray origin (bottom).

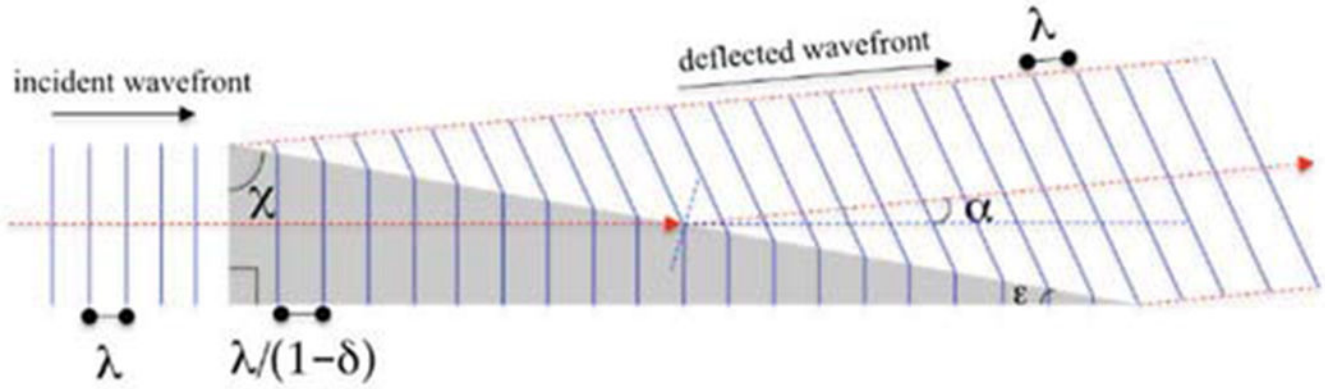

Fig. 2.

Schematic diagram of X-ray beam deflection by a prism, including the X-ray wave length λ, the angle of the bi-prism, the refraction index decrement δ, and the angle of the beam deflection $\alpha = \delta tan\chi$.

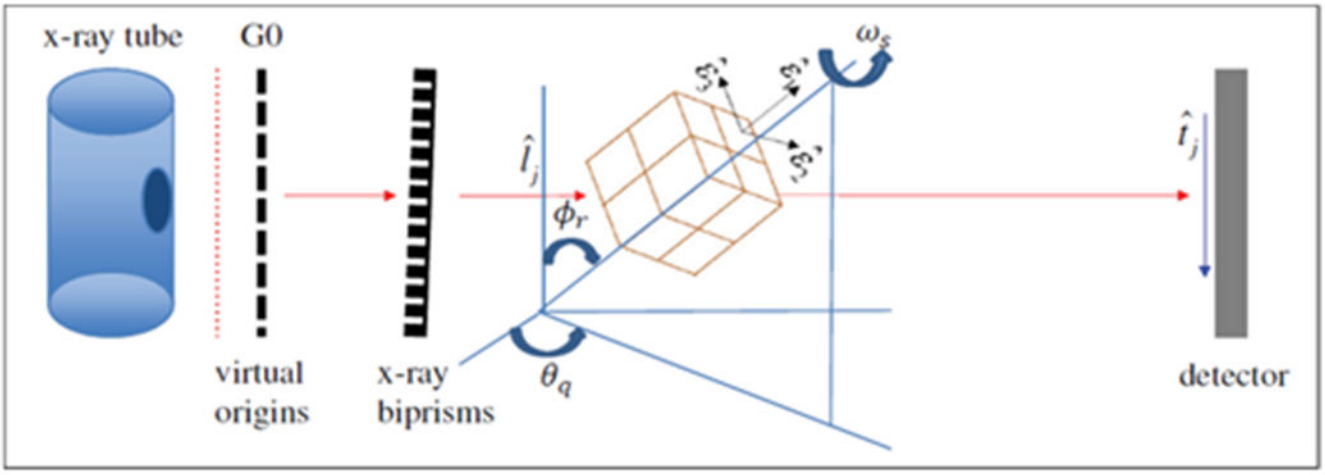

Fig. 3.

Bi-prism-based interferometry. Schematic of the imaging model showing the following unit vectors: $\hat{\epsilon}_1, \hat{\epsilon}_2, \hat{\epsilon}_3 \in \mathbb{R}^3$ are scattering directions (in practice this might be as many as K=17), $\hat{l}_j \in \mathbb{R}^3$ is the direction of the incoming x-ray beam, and $\hat{t}_j \in \mathbb{R}^3$ is the sensitivity direction parallel to the detector surface.

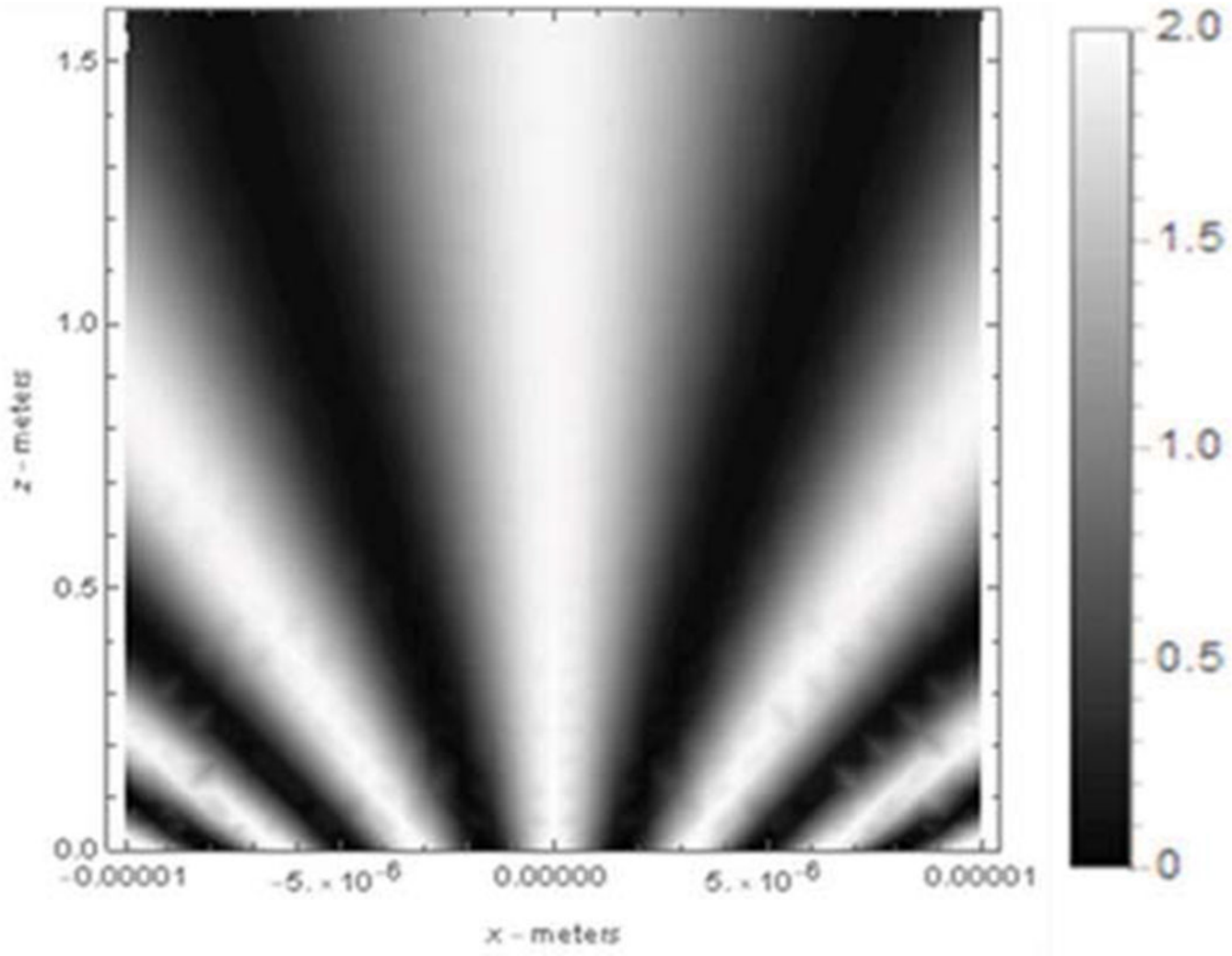

Fig. 4.
One point source with a bi-prism angle of χ=82°.

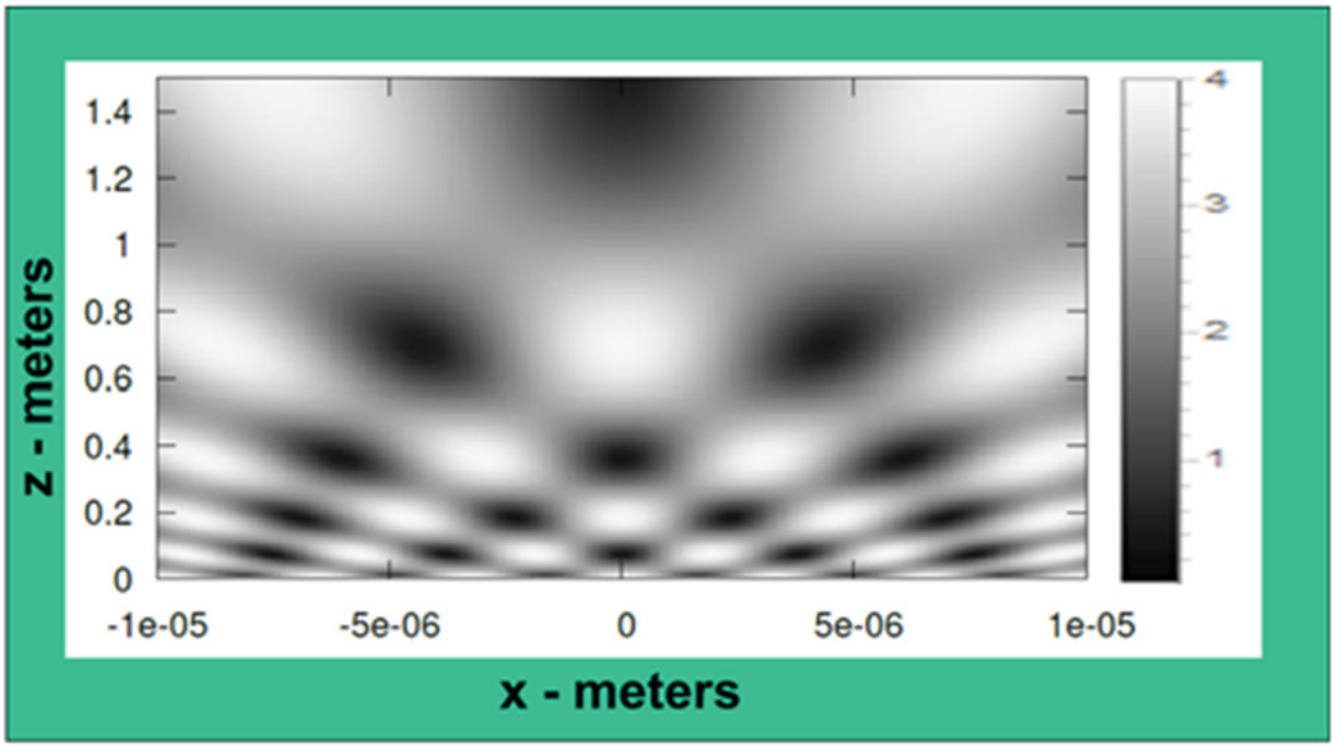

Fig. 5.
Two point sources separated by x_0 = 20 μm with a bi-prism angle of χ=82°.

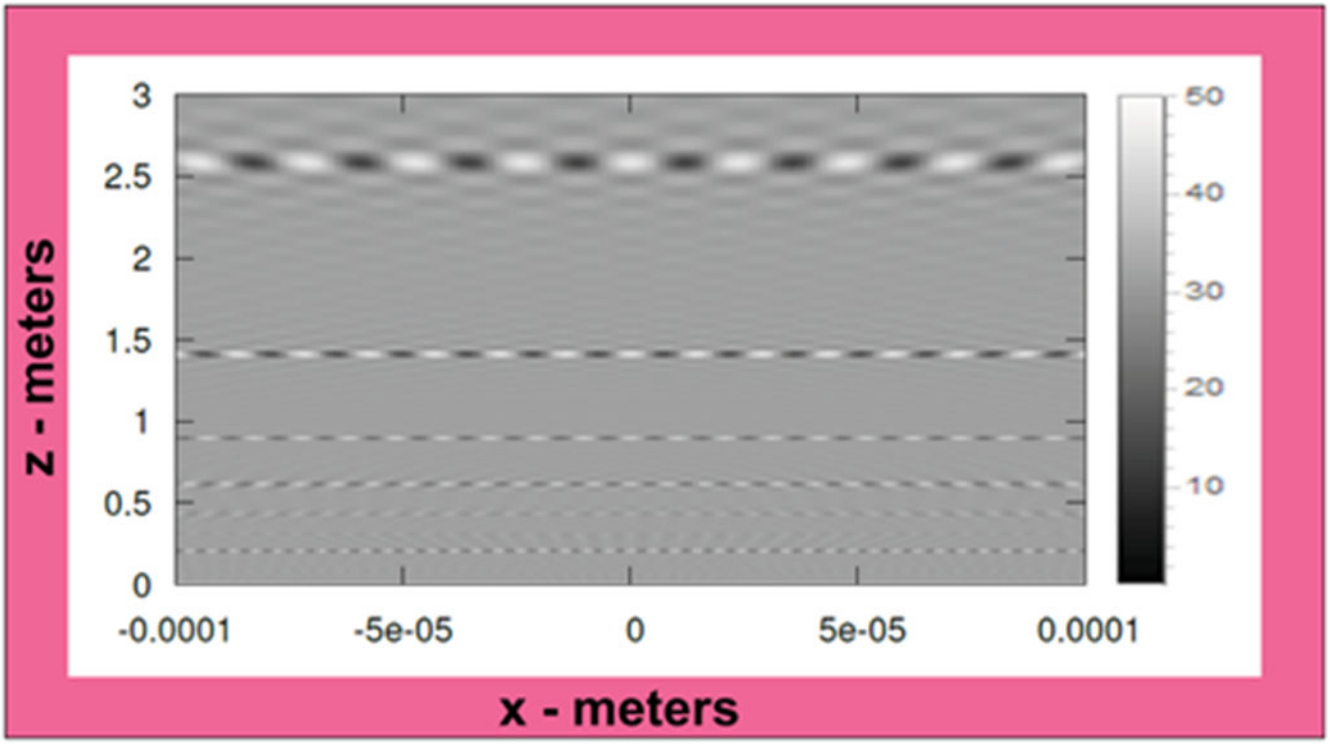

Fig. 6.

25 point sources separated by x_0 = 36.7 μm with a bi-prism angle of χ=82°. Note: Non-periodic fringe visibility.

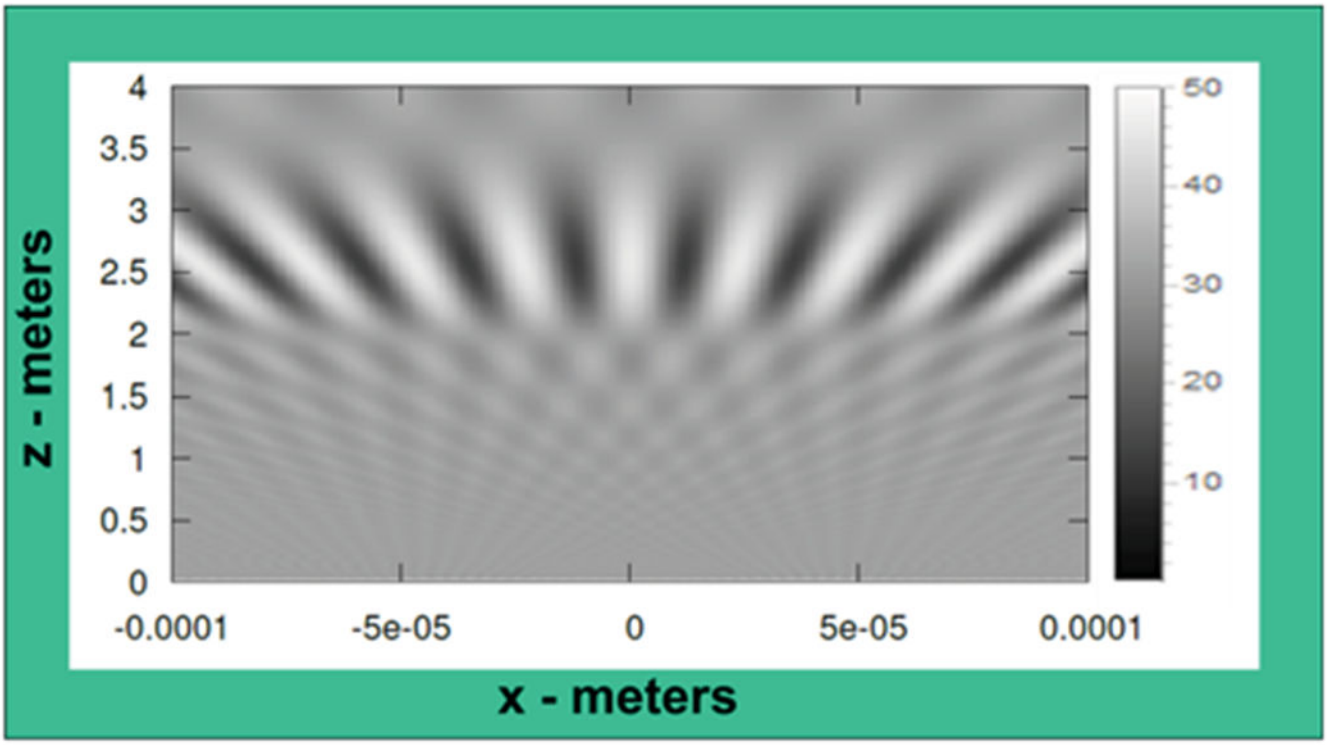

Fig. 7.

25 point sources separated by x_0 = 3.67 μm with a bi-prism angle of χ=82°. Note: Sensitive to reducing the distance between the point sources.

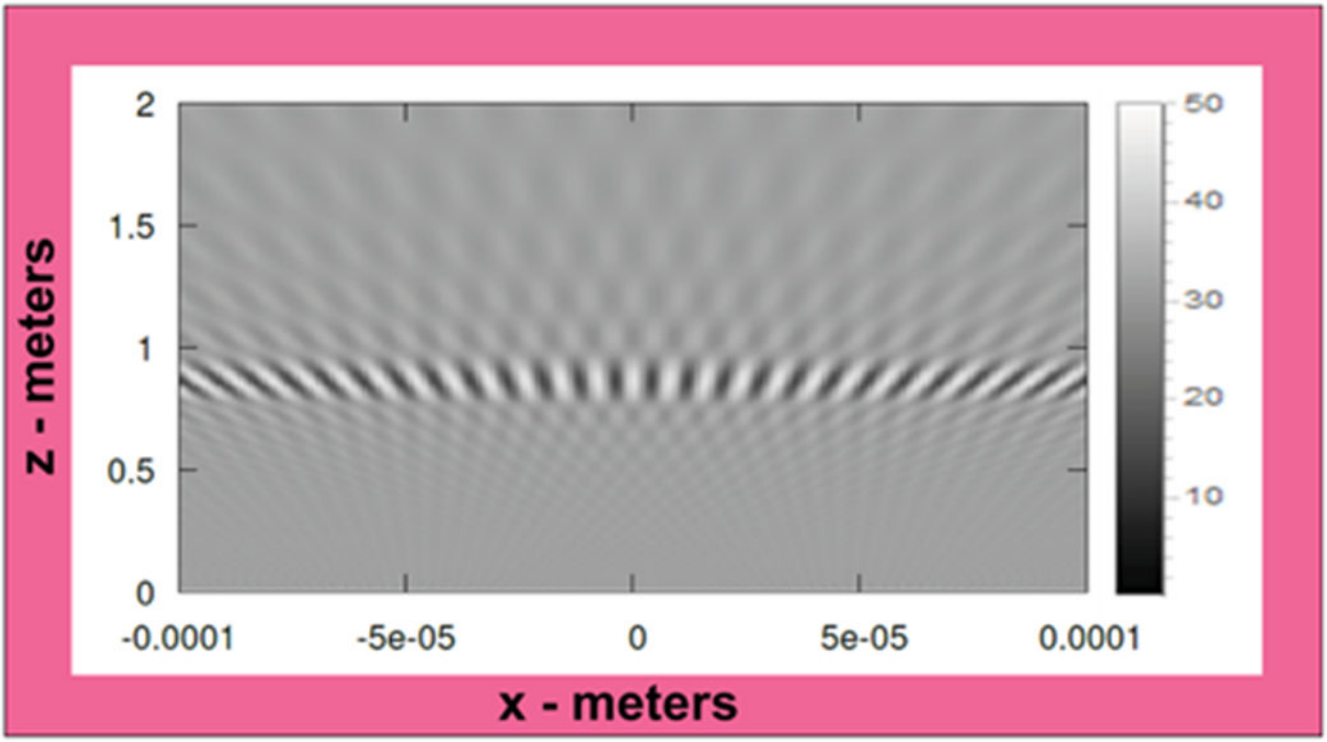

Fig. 8.

25 point sources separated by x_0 = 3.67 ηm with a bi-prism angle of χ=83.67°. Note: Sensitive to small changes in the bi-prism angle.

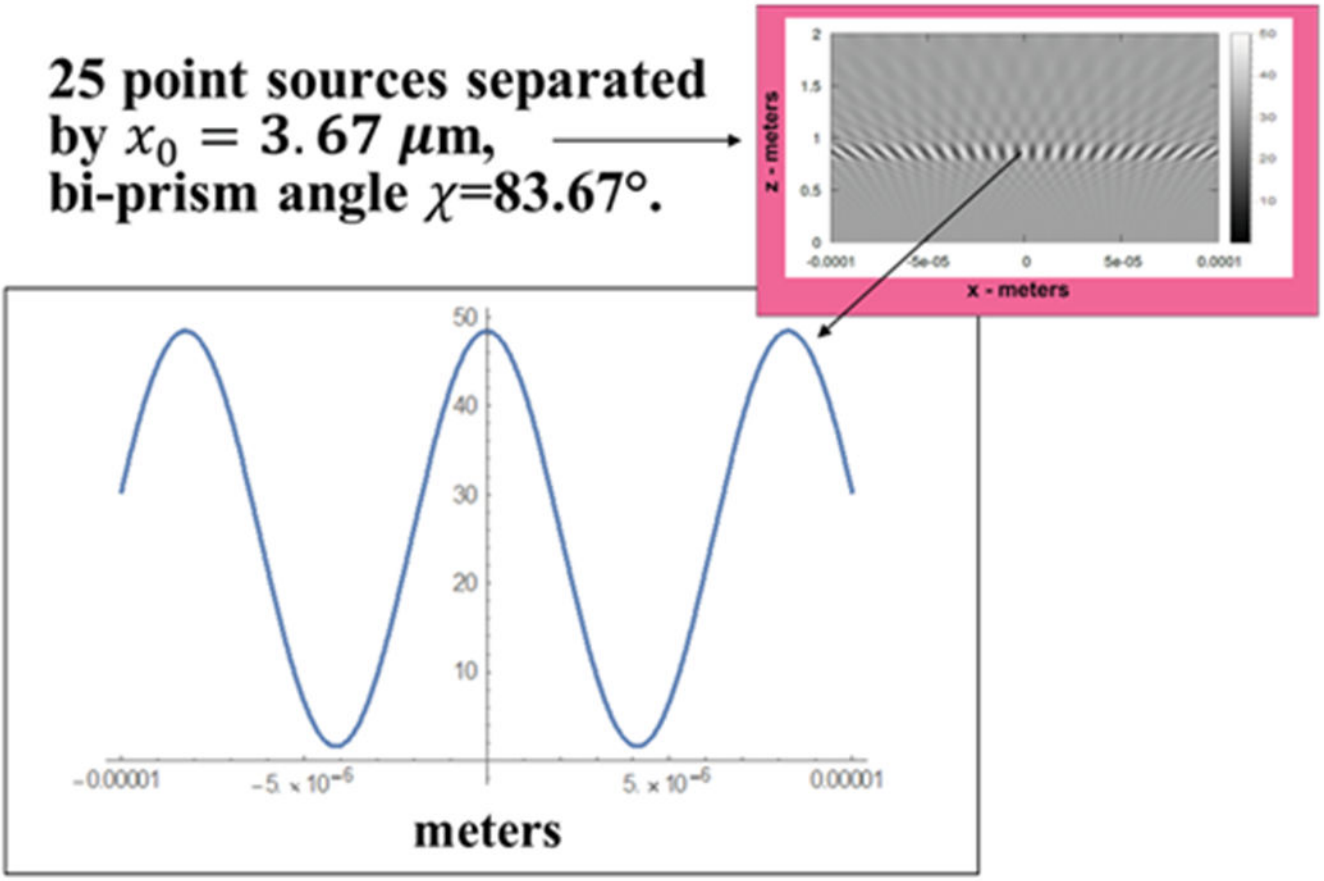

Fig. 9.

Projection of the bi-prism irradiance distribution onto the detector surface at a distance z =0.9 m from the bi-prism that was irradiated by 25 X-ray point sources of wave length λ = 7.1×10^{-11}m (17.5 keV), which are placed at a distance η = 0.4 m in front of the bi-prism.